# Current Correlations in a Quantum Dot Ring: A Role of Quantum Interference

**Bogdan R. Bułka** *[ID] **and Jakub Łuczak** [ID]

Institute of Molecular Physics, Polish Academy of Sciences, ul. M. Smoluchowskiego 17, 60-179 Poznań, Poland; jakub.luczak@ifmpan.poznan.pl
* Correspondence: bogdan.bulka@ifmpan.poznan.pl

**Abstract:** We present studies of the electron transport and circular currents induced by the bias voltage and the magnetic flux threading a ring of three quantum dots coupled with two electrodes. Quantum interference of electron waves passing through the states with opposite chirality plays a relevant role in transport, where one can observe Fano resonance with destructive interference. The quantum interference effect is quantitatively described by local bond currents and their correlation functions. Fluctuations of the transport current are characterized by the Lesovik formula for the shot noise, which is a composition of the bond current correlation functions. In the presence of circular currents, the cross-correlation of the bond currents can be very large, but it is negative and compensates for the large positive auto-correlation functions.

**Keywords:** quantum interference; shot noise; persistent current

## 1. Introduction

In 1985, Webb et al. [1] presented their pioneering experiment, showing Aharonov-Bohm oscillations in a nanoscopic metallic ring and a role of quantum interference (QI) in electron transport. Later, Ji et al. [2] demonstrated the electronic analogue of the optical Mach–Zehnder interferometer (MZI), which was based on closed-geometry transport through single edge states in the quantum Hall regime. Theoretical studies [3–7] predicted coherent transport through single molecules with a ring structure, where, due to their small size, one could show constructive or destructive quantum interference effects at room temperatures. From 2011, these predictions have been experimentally verified, using mechanically controllable break junction (MCBJ) and scanning tunneling microscope break junction (STM-BJ) techniques [8,9] in various molecular systems: Single phenyl, polycyclic aromatic, and conjugated heterocyclic blocks, as well as hydrocarbons (for a recent review on QI in molecular junctions, see [10,11] and the references therein).

Our interest is in the internal local currents and their correlations in a ring geometry to see a role of quantum interference. An interesting aspect is the formation of a quantum vortex flow driven by a net current from the source to the drain electrode, which has been studied in many molecular systems [7,10,12–21] (see also [22]). It has also been shown that, under some conditions, a circular thermoelectric current can exceed the transport current [23]. In particular, our studies focus on the role of the states with opposite chirality in the ring and on the QI effect and the circular current. Correlations of the electron currents (shot noise) through edge states in the Mach–Zehnder interferometer have been extensively studied by Buttiker et al. [24–28] (see also [29] and the references therein). However, in a metallic (or molecular) ring, the situation is different than in the MZI, as multiple reflections are relevant to the formation of the circular current. Our studies will show that the transition from laminar to vortex flow is manifested in the shot noise of local currents. In particular, it will be seen in a

cross-correlation function for the currents in different branches of the ring, which becomes negative and large in the presence of the circular current.

The paper is organized as follows. In the next chapter, Section 2, we will present the model of three quantum dots in a ring geometry, which is the simplest model showing all aspects of QI and current correlations. The model includes a magnetic flux threading the ring, which changes interference conditions as well as inducing a persistent current. The net transport current and the local bond currents, as well as the persistent current (and their conductances), are derived analytically, by means of the non-equilibrium Keldysh Green function technique. It will be shown that the correlation function for the net transport current can be expressed as a composition of the correlation functions for the local currents inside the ring. We will, also, show all shot noise components; in particular, the one for the net transport current (given by Lesovik's formula [30]). The next chapters, Sections 3–5, present the analyses of the results for the case $\Phi = 0$ (without the magnetic flux), for the case with the persistent current only (without the source-drain bias $V$), and for the general case (for $V \neq 0, \Phi \neq 0$) showing the interplay between the bond currents and the persistent current. Finally, in Section 6, the main results of the paper are summarized.

## 2. Calculations of Currents and Their Correlations in Triangular Quantum Dot System

### 2.1. Model

The considered system of three quantum dots (QDs) in an triangular arrangement is presented in Figure 1. This system is described by the Hamiltonian

$$H_{tot} = H_{3QD} + H_{el} + H_{3QD-el}, \tag{1}$$

which consists of parts corresponding to the electrons in the triangular QD system, in the electrodes, and in the coupling between the sub-systems, respectively. The first part is given by

$$H_{3QD} = \sum_{i \in 3QD} \varepsilon_i\, c_i^\dagger c_i + \sum_{i,j \in 3QD} \left( \tilde{t}_{ij} c_i^\dagger c_j + h.c. \right), \tag{2}$$

where the first term describes the single-level energy, $\varepsilon_i$, at the $i$-th QD and the second term corresponds to electron hopping between the QDs. Here, the hopping parameters $\tilde{t}_{12} = t_{12}e^{i\phi/3} = \tilde{t}_{21}^*$, $\tilde{t}_{23} = t_{23}e^{i\phi/3} = \tilde{t}_{32}^*$, and $\tilde{t}_{31} = t_{31}e^{i\phi/3} = \tilde{t}_{13}^*$ include the phase shift $\phi = 2\pi\Phi/(hc/e)$, due to presence of the magnetic flux $\Phi$; where $hc/e$ denotes the one-electron flux quantum. The spin of electrons is irrelevant in our studies and so it is omitted. We consider transport in an open system with the left (L) and right (R) electrodes as reservoirs of electrons, each in thermal equilibrium with a given chemical potential $\mu_\alpha$ and temperature $T_\alpha$. The corresponding Hamiltonian is

$$H_{el} = \sum_{k,\alpha \in L,R} \varepsilon_{k,\alpha}\, c_{k\alpha}^\dagger c_{k\alpha}, \tag{3}$$

where $\varepsilon_{k,\alpha}$ denotes an electron spectrum. The coupling between the 3QD system and the electrodes is given by

$$H_{3QD-el} = \sum_k (t_L\, c_{kL}^\dagger c_1 + t_R\, c_{kR}^\dagger c_2 + h.c.), \tag{4}$$

with tunneling from the electrodes given by the hopping parameters $t_L$ and $t_R$, respectively. The model omits Coulomb interactions and, therefore, one can derive all transport characteristics analytically.
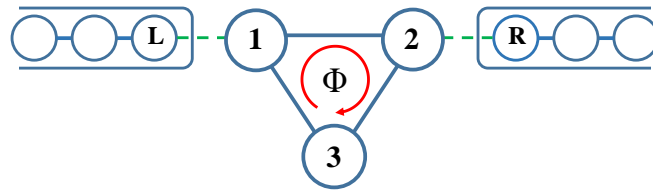
**Figure 1.** Model of the triangular system of three quantum dots (3QDs) threaded by the magnetic flux Φ and attached to the left (L) and the right (R) electrodes.

### 2.2. Calculation of Currents

We consider a steady-state current, with the net transport current through the 3QD system, $I^{tr} = I_{12} + I_{13}$, expressed as a sum of the bond currents through the upper and the lower branches

$$I_{ij} = \frac{e}{\imath\hbar}(\tilde{t}_{ij}\langle c_i^\dagger c_j\rangle - \tilde{t}_{ji}\langle c_j^\dagger c_i\rangle). \tag{5}$$

We use the non-equilibrium Green function technique (NEGF), which is described in many textbooks (e.g., see [31]). To determine the currents, one calculates the lesser Green functions, $G_{ji}^< \equiv \imath\langle c_i^\dagger c_j\rangle$, by means of the equation of motion method (EOM). The coupling with the electrodes is manifested by the lesser Green functions $g_\alpha^< = 2\pi(g_\alpha^r - g_\alpha^a)f_\alpha$, where $g_\alpha^{r,a}$ denotes the retarded (r) and advanced (a) Green functions in the $\alpha$ electrode, and $f_\alpha = 1/(\exp[(E - \mu_\alpha)/k_B T_\alpha] + 1)$ is the Fermi distribution function for an electron with energy $E$, with respect to a chemical potential $\mu_\alpha$ and at temperature $T_\alpha$. For any Green function $G_{ji}^<$, we separate contributions from the left and the right electrodes (i.e., we extract the coefficients in front of $g_L^<$ and $g_R^<$) and, after some algebra, the bond current can be expressed as

$$I_{ij} = -\frac{e}{2\pi\hbar}\int_{-\infty}^{\infty} dE\, [\mathcal{G}_{ij}^L(E)f_L - \mathcal{G}_{ij}^R(E)f_R], \tag{6}$$

where the dimensionless conductances for the upper and the lower branches are

$$\mathcal{G}_{12}^L = 2\Gamma_L t_{12}\Im[d_{23,31}d_{23,23}^*]/A, \tag{7}$$
$$\mathcal{G}_{12}^R = 2\Gamma_R t_{12}\Im[d_{23,31}^* d_{31,31}^*]/A, \tag{8}$$
$$\mathcal{G}_{13}^L = 2\Gamma_L t_{31}\Im[d_{12,23}d_{23,23}^*]/A, \text{ and} \tag{9}$$
$$\mathcal{G}_{13}^R = 2\Gamma_R t_{31}\Im[d_{12,31}d_{23,31}]/A. \tag{10}$$

Here, we denote the coefficients: $d_{12,23} = e^{-\imath\phi}t_{12}t_{23} - t_{31}w_2^r$, $d_{12,31} = t_{12}t_{31} - e^{-\imath\phi}t_{23}w_1^r$, $d_{23,31} = e^{\imath\phi}t_{23}t_{31} - t_{12}w_3$, $d_{23,23} = t_{23}^2 - w_2^r w_3$, $d_{31,31} = t_{31}^2 - w_1^r w_3$, and the denominator

$$A = |w_1^r t_{23}^2 + w_2^r t_{31}^2 + w_3 t_{12}^2 - w_1^r w_2^r w_3 - 2t_{12}t_{23}t_{31}\cos\phi|^2, \tag{11}$$

where $w_1^{r,a} = E - \varepsilon_1 - \gamma_L^{r,a}$, $w_2^{r,a} = E - \varepsilon_2 - \gamma_R^{r,a}$, $w_3 = E - \varepsilon_3$, $\Gamma_\alpha = 2\Im[\gamma_\alpha^a]t_\alpha^2$, and $\gamma_\alpha^{r,a} = g_\alpha^{r,a}t_\alpha^2$.

Note that Equation (6) includes the transport current due to the bias voltage applied to the electrodes, as well as the persistent current induced by the magnetic flux [a term proportional to $\sin\phi$], which can be written as $I_{12} = I_{12}^{tr} - I^\phi$ and $I_{13} = I_{13}^{tr} + I^\phi$, respectively. These coefficients are coupled with those in (7)–(10):

$$\mathcal{G}_{12}^L = \mathcal{G}_{12} - \mathcal{G}_\phi^L, \quad \mathcal{G}_{12}^R = \mathcal{G}_{12} + \mathcal{G}_\phi^R, \tag{12}$$
$$\mathcal{G}_{13}^L = \mathcal{G}_{13} + \mathcal{G}_\phi^L, \quad \mathcal{G}_{13}^R = \mathcal{G}_{13} - \mathcal{G}_\phi^R. \tag{13}$$

The first part is

$$I_{ij}^{tr} = -\frac{e}{2\pi\hbar} \int_{-\infty}^{\infty} dE (f_L - f_R) \mathcal{G}_{ij}(E), \tag{14}$$

where the bond conductances are

$$\mathcal{G}_{12} = \Gamma_L \Gamma_R t_{12} w_3 [t_{23} t_{31} \cos\phi - t_{12} w_3] / A, \text{ and} \tag{15}$$

$$\mathcal{G}_{13} = \Gamma_L \Gamma_R t_{23} [t_{12} t_{31} w_3 \cos\phi - t_{23} t_{31}^2] / A. \tag{16}$$

The net transport current is $I^{tr} = I_{12}^{tr} + I_{13}^{tr}$ and the transmission is given by

$$\mathcal{T} \equiv \mathcal{G}_{12} + \mathcal{G}_{13} = \Gamma_L \Gamma_R [2 t_{12} t_{23} t_{31} w_3 \cos\phi - t_{12}^2 w_3^2 - t_{23}^2 t_{31}^2] / A. \tag{17}$$

The persistent current is expressed as

$$I^\phi \equiv -\frac{e}{\pi\hbar} \int_{-\infty}^{\infty} dE (\mathcal{G}_\phi^L f_L + \mathcal{G}_\phi^R f_R), \tag{18}$$

where

$$\mathcal{G}_\phi^L = \Gamma_L t_{12} t_{23} t_{31} \sin\phi [2 t_{23}^2 - (w_2^a + w_2^r) w_3] / A, \text{ and} \tag{19}$$

$$\mathcal{G}_\phi^R = \Gamma_R t_{12} t_{23} t_{31} \sin\phi [2 t_{31}^2 - (w_1^a + w_1^r) w_3] / A. \tag{20}$$

In the next section, we will show that the voltage bias can induce the circular current, where the bond conductances $\mathcal{G}_{ij}$ are larger than unity or negative.

## 2.3. Calculation of Current Correlations

Here, we consider a single-particle interference effect which takes place in a Mach–Zehnder or Michelson interferometer, but not in a Hanbury Brown and Twiss situation with a two-particle interference effect. The current fluctuations are described by the operator $\Delta \hat{I}_{ij}(t) - \langle \hat{I}_{ij}(t) \rangle$, and the current–current correlation function is defined as [32]

$$S_{ij,nm}(t, t') \equiv \frac{1}{2} \left[ \langle \hat{I}_{ij}(t) \hat{I}_{nm}(t') + \hat{I}_{nm}(t') \hat{I}_{ij}(t) \rangle - 2\langle \hat{I}_{ij}(t) \langle \hat{I}_{nm}(t') \rangle \right]. \tag{21}$$

We consider the steady currents, for which the correlation functions can be represented, in the frequency domain, by their spectral density

$$S_{ij,nm}(\omega) \equiv 2 \int_{-\infty}^{\infty} d\tau e^{i\omega\tau} S_{ij,nm}(\tau). \tag{22}$$

In this work, we shall restrict ourselves to studying the current correlations at the zero-frequency limit $\omega = 0$. As the net transport current is $\hat{I}^{tr} = \hat{I}_{12} + \hat{I}_{13}$, its current correlation function can be expressed as a composition of the correlation functions for the bond currents

$$S_{tr,tr} = S_{12,12} + S_{13,13} + 2S_{12,13}. \tag{23}$$

The correlation functions $S_{ij,in}$ can be derived by means of Wick's theorem [31] and are expressed as

$$S_{ij,in} = \frac{e^2}{\pi\hbar} \frac{1}{2} \{ t_{ij} t_{in} (\langle c_i^\dagger c_j \rangle \langle c_i c_n^\dagger \rangle + \langle c_i^\dagger c_n \rangle \langle c_i c_j^\dagger \rangle)) - t_{ij} t_{ni} (\langle c_i^\dagger c_i \rangle \langle c_n c_j^\dagger \rangle + \langle c_n^\dagger c_j \rangle \langle c_i c_i^\dagger \rangle)) $$
$$+ t_{ji} t_{ni} (\langle c_j^\dagger c_i \rangle \langle c_n c_i^\dagger \rangle + \langle c_n^\dagger c_i \rangle \langle c_j c_i^\dagger \rangle)) - t_{ji} t_{in} (\langle c_i^\dagger c_i \rangle \langle c_j c_n^\dagger \rangle + \langle c_j^\dagger c_n \rangle \langle c_i c_i^\dagger \rangle)) \}. \tag{24}$$

Once again, we use the NEGF method. As the lesser Green functions, $G_{ji}^< \equiv \imath \langle c_i^\dagger c_j \rangle$, and the greater Green functions, $G_{ij}^> \equiv -\imath \langle c_i c_j^\dagger \rangle$, have the same structure, one should only exchange the Green functions in the electrodes: $g_\alpha^< = 2\pi(g_\alpha^r - g_\alpha^a)f_\alpha \leftrightarrow g_\alpha^> = -2\pi(g_\alpha^r - g_\alpha^a)(1 - f_\alpha)$. Separating coefficients in front of $f_L(1 - f_L)$, $f_R(1 - f_R)$, and $f_L(1 - f_R) + f_R(1 - f_L)$, and after some algebra, one can derive a compact formula for any current–current function. The auto-correlation function for the net transport current is given by the well-known Lesovik formula [30,33,34] (see also [32,35] for a multi-terminal and multi-channel case)

$$S_{tr,tr} = \frac{e^2}{\pi\hbar} \int_{-\infty}^{\infty} dE \left\{ \mathcal{T}^2 \left[ f_L(1 - f_L) + f_R(1 - f_R) \right] + \mathcal{T}(1 - \mathcal{T}) \left[ f_L(1 - f_R) + f_R(1 - f_L) \right] \right\}, \quad (25)$$

where $\mathcal{T}$ is the transmission through the 3QD system. For a given temperature $T_L = T_R = T$, one has $f_L(1 - f_R) + f_R(1 - f_L) = \coth[(\mu_L - \mu_R)/2k_BT](f_L - f_R)$ and, thus,

$$S_{tr,tr} = 2I^{tr} \coth\left(\frac{eV}{2k_BT}\right) - \frac{e^2}{\pi\hbar} \int_{-\infty}^{\infty} dE \, \mathcal{T}^2 \left( f_L - f_R \right)^2. \quad (26)$$

When the scale of the energy dependence $\Delta E$ of the transmission $\mathcal{T}$ is much larger than both the temperature and applied voltage (i.e., $\Delta E \gg eV \gg k_BT$), one can obtain the well known explicit relation (see Blanter and Buttiker [32])

$$S_{tr,tr} = \frac{e^2}{\pi\hbar} \left[ 2k_BT \, \mathcal{T}^2(E_F) + eV \coth\left(\frac{eV}{2k_BT}\right) \mathcal{S}_{tr,tr}^{sh} \right]. \quad (27)$$

The first term is the Nyquist-Johnson noise at equilibrium and the second term, with $\mathcal{S}_{tr,tr}^{sh} = \mathcal{T}(E_F)(1 - \mathcal{T}(E_F))$, corresponds to the shot noise [30,32,34].

The correlation functions for the bond currents are calculated from Equation (24) and are expressed as

$$S_{ij,ik} = \frac{e^2}{\pi\hbar} \int_{-\infty}^{\infty} dE \left\{ \mathcal{S}_{ij,ik}^{sh} \left[ f_L(1 - f_R) + f_R(1 - f_L) \right] + \left[ \mathcal{G}_{ij}^L \mathcal{G}_{ik}^L f_L(1 - f_L) + \mathcal{G}_{ij}^R \mathcal{G}_{ik}^R f_R(1 - f_R) \right] \right\}, \quad (28)$$

where $\mathcal{G}_{ij}^\alpha$ are given by (7)–(10), and the dimensionless spectral functions of the shot noise components are

$$\mathcal{S}_{12,12}^{sh} = \Gamma_L\Gamma_R t_{12}^2 |d_{23,31}^2 - d_{23,23}d_{31,31}^*|^2/A^2, \quad (29)$$

$$\mathcal{S}_{13,13}^{sh} = \Gamma_L\Gamma_R t_{31}^2 |d_{12,23}^* d_{23,31} + d_{12,31}d_{23,23}^*|^2/A^2, \quad (30)$$

$$\mathcal{S}_{12,13}^{sh} = \Gamma_L\Gamma_R t_{12}t_{31} \Re[(d_{23,31}^2 - d_{23,23}d_{31,31}^*)(d_{12,23}^* d_{23,31}^* + d_{12,31}d_{23,23}^*)]/A^2, \text{ and} \quad (31)$$

$$\mathcal{S}_{tr,tr}^{sh} \equiv \mathcal{S}_{12,12}^{sh} + \mathcal{S}_{13,13}^{sh} + 2\mathcal{S}_{12,13}^{sh} = \Gamma_L\Gamma_R |t_{12}(d_{23,31}^2 - d_{23,23}d_{31,31}^*) + t_{31}(d_{12,23}d_{23,31} + d_{12,31}^* d_{23,23})|^2/A^2. \quad (32)$$

## 3. Bond Currents and Their Correlations: Driven Circular Current in the Case of $\Phi = 0$

Let us analyse the bond currents in detail; first in the absence of the magnetic flux, $\Phi = 0$, and for a linear response limit $V \to 0$. Using the derivations from the previous section, one can easily calculate the bond conductances and current correlation functions. The results are presented in Figure 2 for an equilateral triangle 3QD system (with all inter-dot hopping parameters $t_{12} = t_{23} = t_{31} = -1$, which is taken as unity in our further calculations) and for various values of the energy level $\varepsilon_3$ at the 3rd QD. The central column corresponds to the case $\varepsilon_1 = \varepsilon_2 = \varepsilon_3 = 0$, when the eigenenergies are given by $E_k = 2t \cos k$, for the wave-vector $k = 0$ and the degenerate state for $k = \pm 2\pi/3$. It can be seen in the transmission (black curve), which is equal to $\mathcal{T} = 1$ at $E = -2$ and $\mathcal{T} = 0$ at $E = 1$, where the Fano resonance takes place, with destructive interference of two electron waves. At low $E < 0$, the incoming wave from the left electrode is split into two branches and the bond conductances are positive, $0 \le \mathcal{G}_{12}, \mathcal{G}_{13} \le 1$ (see the blue and green curves in the top panel of Figure 2). The cross-correlation

function $\mathcal{S}_{12,13}^{sh}$ (for the currents in both branches) is positive (see the red curve in the bottom panel in Figure 2). Note that, at the lowest resonant level, all correlation functions $\mathcal{S}_{12,12}^{sh} = \mathcal{S}_{13,13}^{sh} = \mathcal{S}_{12,13}^{sh} = 0$, which means that the currents in both branches are uncorrelated.

For $E > 0$, the conductances $\mathcal{G}_{12}$ and $\mathcal{G}_{13}$ can be negative and exceed unity (with their maximal absolute values inversely proportional to the coupling $\Gamma_\alpha$). This manifests a circular current driven by injected electronic waves to the 3QD system, which can not reach the drain electrode; therefore, they are reflected backwards to the other branch of the ring. The circular current can be characterized by the conductance (see also [16])

$$\mathcal{G}^{dr} \equiv \begin{cases} \mathcal{G}_{12} & \text{for } \mathcal{G}_{12} < 0, \\ -\mathcal{G}_{13} & \text{for } \mathcal{G}_{13} < 0, \end{cases} \tag{33}$$

where the superscript "*dr*" marks the contribution to the circular current driven by the bias voltage, in order to distinguish it from the persistent current induced by the flux (which will be analysed later). There is some ambiguity in definition of the circular current. Our definition (33) is similar to the one given by the condition sign[$\mathcal{G}_{12}$] = $-$sign[$\mathcal{G}_{13}$] for the vortex flow, used by Jayannavar and Deo [36] and Stefanucci et al. [16] (see [37]–which refers to [7] ).
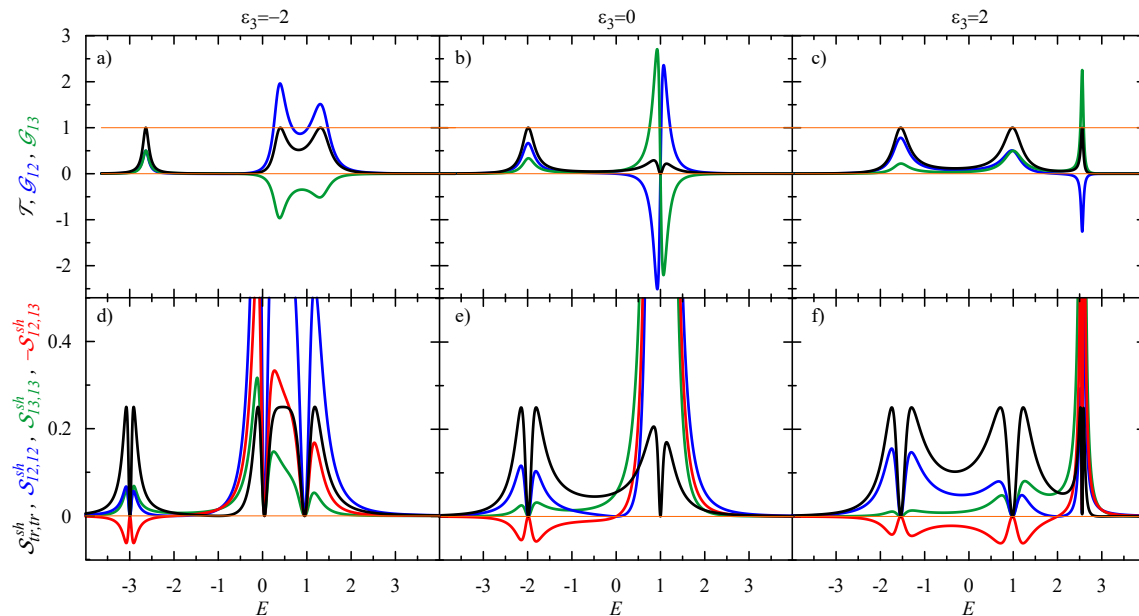


**Figure 2.** (Top) Transmission and dimensionless bond conductances: $\mathcal{T}$—black, $\mathcal{G}_{12}$—blue, and $\mathcal{G}_{13}$—green. (Bottom) Dimensionless spectral function of the shot noise: $\mathcal{S}_{tr,tr}^{sh}$—black, $\mathcal{S}_{12,12}^{sh}$—blue, $\mathcal{S}_{13,13}^{sh}$—green, and $-\mathcal{S}_{12,13}^{sh}$—red; calculated as a function of the electron energy $E$ for the equilateral triangle system of 3QDs (with the inter-dot hopping $t_{12} = t_{23} = t_{31} = -1$, which is taken as unity in this paper) in the linear response limit $V \to 0$. The dot levels are $\varepsilon_1 = \varepsilon_2 = 0$ and $\varepsilon_3 = -2, 0, 2$, for left, center, and right columns, respectively. The coupling with the electrodes is taken to be $\Gamma_L = \Gamma_R = 0.25$. Note that the cross-correlation function $\mathcal{S}_{12,13}^{sh}$ (red) is plotted negatively to show the zero crossing more clearly.

For the considered case in Figure 2b, with $\varepsilon_3 = 0$, the circular current is driven counter-clockwise for $0 < E < 1$ and changes its direction to clockwise at the degeneracy point, $E = 1$ (i.e., when $\mathcal{G}_{13}$ becomes negative). All correlation functions are large in the presence of the circular current; their maximum is inversely proportional to $\Gamma_\alpha^2$. The cross-correlation $\mathcal{S}_{12,13}^{sh}$ is large but negative and, therefore, this component reduces the transport shot noise, $\mathcal{S}_{tr,tr}^{sh} = \mathcal{S}_{12,12}^{sh} + \mathcal{S}_{13,13}^{sh} + 2\mathcal{S}_{12,13}^{sh}$ to the Lesovik formula $\mathcal{T}(1 - \mathcal{T})$, which reaches zero at the degeneracy point $E = 1$ (see the black curve in Figure 2e).

This situation is similar to multi-channel current correlations in transport through a quantum dot connected to magnetic electrodes [38], where cross-correlations for currents of different spins usually reduce the total shot noise to a sub-Poissonian noise with Fano factor $F < 1$ (however, in the presence of Coulomb interactions, the cross-correlations can be positive and lead to a super-Poissonian shot noise with $F > 1$).

The plots on the left and right hand sides of Figure 2 give more insight into the circular current effect. They are calculated for the dot level $\varepsilon_3 = \mp 2$ shifted by a gate potential, which breaks the symmetry of the system and removes the degeneracy of the states. Three resonant levels can be observed with $\mathcal{T} = 1$, where two of them are shifted to the left/right for $\varepsilon_3 = \mp 2$; however, the state at $E = 1$ is unaffected. There is still mirror symmetry, for which one gets three eigenstates, where two of them are linear compositions of all local states, but the one at $E = 1$ has the eigenvector $1/\sqrt{2}(c_1^\dagger - c_2^\dagger)|0\rangle$, which is separated for the 3rd QD. Therefore, the bond currents are composed of the currents through all three eigenstates, and their contribution depends on $E$. From these plots, one can see that the circular current is driven, for $E > \varepsilon_3$, when the cross-correlation $\mathcal{S}_{12,13}^{sh}$ becomes negative. The direction of the current depends on the position of the eigenlevels and their current contributions. For $\varepsilon_3 = -2$, the current circulates clockwise, whereas its direction is counter-clockwise for $\varepsilon_3 = 2$.

Here, we assumed a flat band approximation (FBA) for the electronic structure in the electrodes (i.e., the Green functions $g_\alpha^{r,a} = \mp \iota \pi \rho$, where $\rho$ denotes the density of states). Appendix A presents analytical results for the currents and shot noise in the fully-symmetric 3QD system coupled to a semi-infinite chain of atoms. The results are qualitatively similar. However, the FBA is more convenient for the analysis than the system coupled to atomic chains; in particular, for the cases with $\varepsilon_3 = \mp 2$, when localized states appear at $-2.99$ and $2.56$ (i.e., below/above the energy band of the atomic chain).

The above analysis was performed under the assumption of a smooth energy dependence of the conductance in the small voltage limit $V \to 0$ and at $T = 0$. However, the conductances exhibit sharp resonant characteristics in the energy scale $\Delta E \propto \Gamma_\alpha$ and, therefore, one can expect that these features will be smoothed out with an increase of voltage bias and temperature. Figure 3 presents the Fano factor $F = S_{tr,tr}/2eI^{tr}$, which is the ratio of the current correlation function to the net transport current, which was calculated numerically from Equations (17) and (26). At $E = -2$, one can observe the evolution from the coherent regime, from $F = 0$ to $F = 1/2$ in the sequential regime, for $eV \gg \Gamma_\alpha$ or $k_B T \gg \Gamma_\alpha$. Quantum interference plays a crucial role at $E = 1$, leading to the Fano resonance for which the transmission $\mathcal{T} = 0$ and $F = 1$ in the low voltage/temperature regime. An increase of the voltage/temperature results only in a small reduction of the Fano factor.
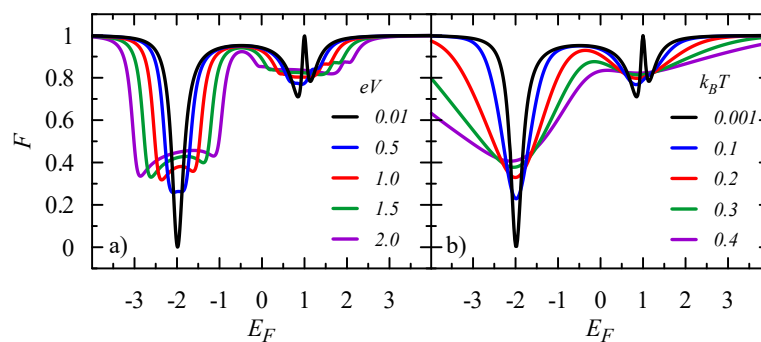


**Figure 3.** Fano factor as a function of the Fermi energy $E_F$ for the equilateral triangle 3QDs system ($t_{12} = t_{23} = t_{31} = -1$ and $\varepsilon_1 = \varepsilon_2 = \varepsilon_3 = 0$) (**a**) for various bias voltages $eV = 0.01, 0.5, 1.0, 1.5,$ and 2.0, at $T = 0$; and (**b**) for various temperatures $k_B T = 0.001, 0.1, 0.2, 0.3,$ and 0.4, for $V \to 0$. The coupling to the electrodes is taken as $\Gamma_L = \Gamma_R = 0.25$, and the chemical potentials in the electrodes are $\mu_L = E_F - eV/2$ and $\mu_R = E_F + eV/2$.

## 4. Persistent Current and Its Noise: The Case $V = 0$

The persistent current and its noise has been studied in many papers (e.g., by Büttiker et al. [39–42], Semenov and Zaikin [43–46], Moskalates [47], and, more recently, by Komnik and Langhanke [48]) using full counting statistics (FCS), as well as in 1D Hubbard rings by exact diagonalization by Saha and Maiti [49] (see, also, the book by Imry [50]).

Here, we briefly present the results for the persistent current and shot noise in the triangle of 3QDs. Notice that, in the considered case, the phase coherence length of electrons is assumed to be larger than the ring circumference, $L_\phi \gg L$ [51]. The circular current is given by Equation (18), which shows that all electrons, up to the chemical potential in the electrodes, are driven by the magnetic flux $\Phi$. Figure 4 exhibits the plots of $I^\phi$, derived from Equation (18), for different couplings with the electrodes. In the weak coupling limit, where $\Gamma \to 0$ and the perfect ring is embedded in the reservoir, the persistent current can be simply expressed as

$$I^\phi = e \sum_k v_k f_k = -\frac{e}{\hbar} \sum_k 2t \sin(k + \phi/3) f_k \,, \tag{34}$$

where $f_k = 1/(\exp[(E_F - E_k)/k_B T] + 1)$ is the Fermi distribution for the electron with wave-vector $k$, energy $E_k = 2t \cos(k + \phi/3)$, and velocity $v_k = (1/\hbar)\partial E_k/\partial k = (-2t/\hbar) \sin(k + \phi/3)$, and where $\phi = 2\pi\Phi/(hc/e)$ is the phase shift due to the magnetic flux $\Phi$. The sum runs over $k = 2\pi n/(Na)$ for $n = 0, \pm 1$, where $N = 3$ and $a = 1$ is the distance between the sites in the triangle. The current correlator is derived from Equation (24)

$$S_{\phi,\phi} = \frac{e^2}{\hbar} \sum_k 4t^2 \sin^2(k + \phi/3) f_k (1 - f_k) \,. \tag{35}$$

This result says that fluctuations of the persistent current could occur when the number of electrons in the ring fluctuates (i.e., an electron state moves through the Fermi level and $I^\phi$ jumps). We show, below, that the coupling with the electrodes (as a dissipative environment) results in current fluctuations [40,41], as well.
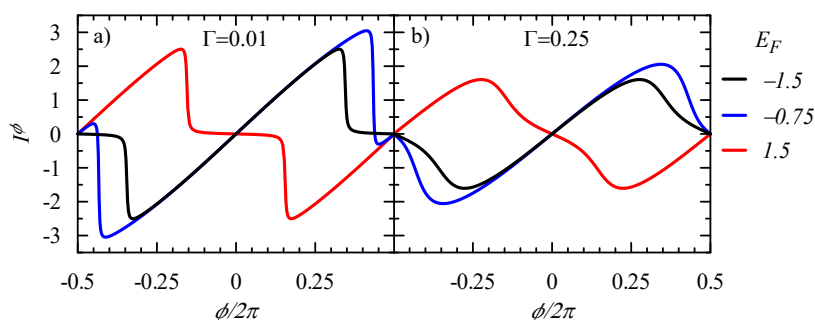


**Figure 4.** Persistent current $I^\phi$ versus the flux $\phi$ threading the equilateral triangle system of 3QDs ($t_{12} = t_{23} = t_{31} = -1$ and $\varepsilon_1 = \varepsilon_2 = \varepsilon_3 = 0$). The coupling is taken as $\Gamma_L = \Gamma_R = \Gamma = 0.01$ and $0.25$; the Fermi energies are $E_F = -1.5$ (**black**), $-0.75$ (**blue**), $1.5$ (**red**); and $T = 0$.

At the limit, $V \to 0$, the integrand function of the noise $S_{ij,in}$, Equation (28), is proportional to $f(E)(1 - f(E))$, which becomes the Dirac delta for $T \to 0$ and, therefore, one can analyze the spectral function $S_{\phi,\phi} = S_{12,12} + S_{13,13} - 2S_{12,13}$, where the components are $S_{ij,in} = S_{ij,in}^{sh} + G_{ij}^L G_{in}^L + G_{ij}^R G_{in}^R$ (see Equations (7)–(10) and (29)–(31)). Figure 5 presents the correlation function $S_{\phi,\phi}$ and its various components for the Fermi energy $E_F = -1.5$ and the strong coupling $\Gamma_L = \Gamma_R = 1$ when fluctuations are large. Notice that the fluctuations of the bond currents $S_{12,12}$ and $S_{13,13}$ (the blue and green curves, respectively) are different, although the average currents are equal. The cross-correlation function $S_{12,13}$ is positive at $\phi = 0$, but it becomes negative for larger $\phi$, due to the quantum interference between electron waves passing through different states (as described in the previous section).

Figure 5 also shows $(\mathcal{G}_{12}^L)^2$ (blue-dashed curve) and $(\mathcal{G}_{12}^L)^2$ (blue-dotted curve), which correspond to the local fluctuations of the injected/ejected currents to/from the upper branch on the left and right junctions, respectively (see Equation (28)). The magnetic flux breaks the symmetry, inducing the persistent current and, therefore, the local conductances $\mathcal{G}_{12}^L$ and $\mathcal{G}_{12}^R$ are asymmetric.
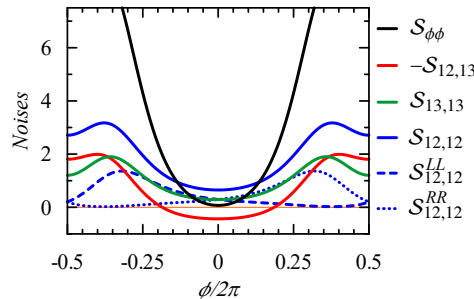


**Figure 5.** Flux dependence of spectral function of the persistent current correlator $\mathcal{S}_{\phi,\phi}$ (**black**) and its components: $\mathcal{S}_{12,12}$ (**blue**), $\mathcal{S}_{13,13}$ (**green**), $-\mathcal{S}_{12,13}$ (**red**), and $\mathcal{S}_{12,12}^{LL} = (\mathcal{G}_{12}^L)^2$ (**blue-dashed**), $\mathcal{S}_{12,12}^{RR} = (\mathcal{G}_{12}^R)^2$, (**blue-dotted**), respectively. We assume strong coupling: $\Gamma_L = \Gamma_R = 1.0$, $E_F = -1.5$, and $T = 0$.

## 5. Correlation of Persistent and Transport Currents, $\Phi \neq 0$ and $V \neq 0$

In this section, we analyze the currents and their correlations in the general case, derived from Equations (6), (14), (18), and (28), in the presence of voltage bias and magnetic flux. The results for the conductances and the spectral functions of the shot noise are presented in Figure 6. The magnetic flux splits the degenerated levels at $E = 1$ and destroys the Fano resonance. Figure 6a shows that there is no destructive interference for a small flux $\phi = 2\pi/16$, and the transmission is $\mathcal{T} = 1$ for all resonances. One can observe the driven circular current for $E > 0$, with negative $\mathcal{G}_{12}$ and $\mathcal{G}_{13}$, but their amplitudes are much lower than in the absence of the flux (compare with Figure 2b for $\phi = 0$). For a larger flux, $\phi = 2\pi/4$, there is no driven component of the circular current (see Figure 6b, where $\mathcal{G}_{12}$, $\mathcal{G}_{13} \geq 0$). It can also be seen that, for the state at $E = 0$, the electronic waves pass only through the lower branch of the ring, and the upper branch is blocked (with $\mathcal{G}_{13} = 1$ and $\mathcal{G}_{12} = 0$, respectively).
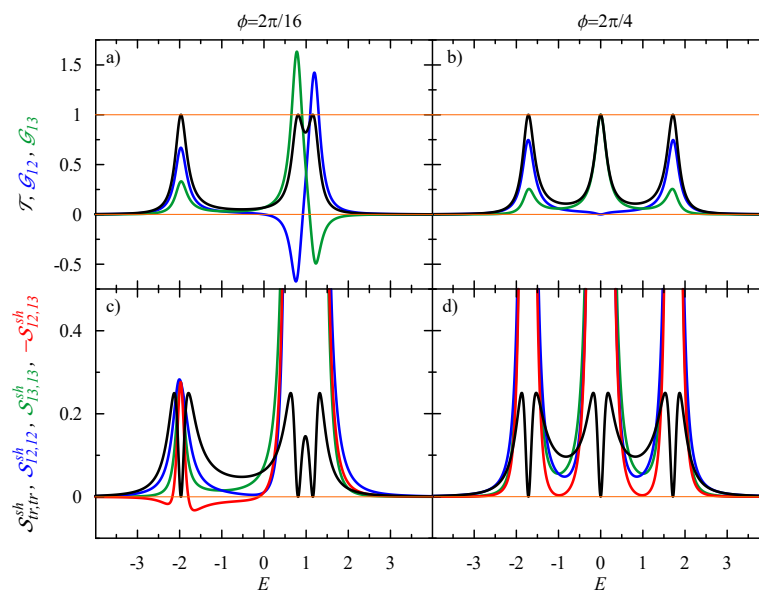


**Figure 6.** (**Top**) Energy dependence of driven conductance $\mathcal{G}_{12}$ (blue), $\mathcal{G}_{13}$ (**green**) and transmission $\mathcal{T}$ (**black**). (**Bottom**) Shot noise $\mathcal{S}_{tr,tr}^{sh}$ (**black**) with the components: $\mathcal{S}_{12,12}^{sh}$ (**blue**), $\mathcal{S}_{13,13}^{sh}$ (**green**), and $-\mathcal{S}_{12,13}^{sh}$ (**red**) for the considered triangular 3QD system threaded by the flux $\phi = 2\pi/16$ (**left**) or $\phi = 2\pi/4$ (**right**); the coupling is $\Gamma_L = \Gamma_R = 0.25$, and $T = 0$. Note that we plot $-\mathcal{S}_{12,13}^{sh}$.

The lower panel of Figure 6 presents the spectral functions of the shot noise. According the Lesovik formula, $\mathcal{S}^{sh}_{tr,tr} = 0$ at the resonant states (as $\mathcal{T} = 1$). This seems to be similar to the case $\phi = 0$ presented in the lower panel in Figure 2. However, there is a great difference in the components of the shot noise $\mathcal{S}^{sh}_{ij,in}$, indicating the different nature of transport through these states and the role of quantum interference. Let us focus on the lowest resonant state, at $E = -2$, in Figure 6c, and compare with that in Figure 2e, in the absence of the flux. In the former case, the currents in both branches were uncorrelated, and $\mathcal{S}^{sh}_{12,12} = \mathcal{S}^{sh}_{13,13} = \mathcal{S}^{sh}_{12,13} = 0$. In the presence of the flux, quantum interference becomes relevant, which is seen in the shot noise (Figure 6c). Now, the currents in both branches are correlated; $\mathcal{S}^{sh}_{12,13}$ is negative close to resonance and fully compensates for the positive contributions $\mathcal{S}^{sh}_{12,12}$ and $\mathcal{S}^{sh}_{13,13}$ at resonance. For $\phi = 2\pi/4$ (see Figure 6d), all shot noise components are large, which indicates a strong quantum interference effect.

Figure 7 shows the Fano factor in the presence of the flux $\phi = 2\pi/16$ and for various bias voltages. Compared with the results in Figure 3 for $\phi = 0$, one can see how a small flux can destroy quantum interference and change electron transport. It is particularly seen close to $E = -1$, where the states with opposite chirality are located. In the case $\phi = 0$, one can observe the Fano resonance with a perfect destructive interference, $\mathcal{T} = 0$ and $F = 1$. With an increase of the flux $\phi$, the Fano dip disappears, the two states are split, and transmission reaches its maximum value $\mathcal{T} = 1$; the Fano factor $F = 0$ when the splitting $\Delta E > \Gamma_\alpha$. A similar effect was seen in the case of Figure 2, where a change of the position of the local level $\varepsilon_3$ removed the state degeneracy and destroyed the Fano resonance.
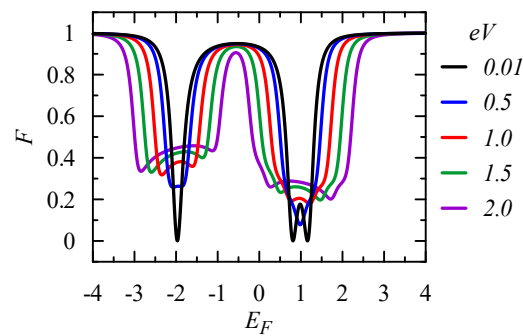


**Figure 7.** Fano factor as a function of $E_F$ for the considered 3QD system threaded by the flux $\phi = 2\pi/16$ and for various bias voltages $eV = 0.01, 0.5, 1.0, 1.5,$ and $2.0$. The coupling is $\Gamma_L = \Gamma_R = 0.25$, the chemical potentials are $\mu_L = E_F - eV/2$ and $\mu_R = E_F + eV/2$, and $T = 0$.

For the strong coupling $\Gamma_L = \Gamma_R = 1$, the intensity of the transport current is comparable to the persistent current and, therefore, one can expect a significant driven circular current. Figure 8 presents the flux dependence of the total circular current $I^c$ and its driven component $I^{dr}$, as well as the transport current $I^{tr}$, for various voltages. For the considered case $E_F = 0.9$, the driven current circulates counter-clockwise and deforms the flux dependence of the circular currents, which become asymmetric.
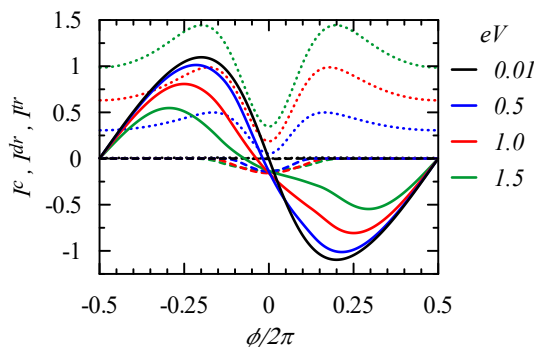
**Figure 8.** Circular current $I^c = I^{dr} + I^{\phi}$ (solid curves), its driven component $I^{dr}$ (dashed curves), and the net transport current $I^{tr}$ (dotted curves) versus $\phi$ for various bias voltages: $eV = 0.01$, 0.5, 1.0, and 1.5. We assume a strong coupling $\Gamma_L = \Gamma_R = 1$, the chemical potentials are $\mu_L = E_F - eV/2$, $\mu_R = E_F + eV/2$, $E_F = 0.9$, and $T = 0$.

## 6. Summary

We considered the influence of quantum interference on electron transport and current correlations in a ring of three quantum dots threaded by a magnetic flux. We assumed non-interacting electrons and calculated the bond conductances, the local currents, and the current correlation functions—in particular, the shot noise—by means of the non-equilibrium Keldysh Green function technique, taking into account multiple reflections of the electron wave inside the ring. As we considered elastic scatterings, for which Kirchhoff's current law is fulfilled, the transmission $\mathcal{T} = \mathcal{G}_{12} + \mathcal{G}_{13}$ is a sum of the local bond conductances and the shot noise for the transport current is a composition of the local current correlation functions, $\mathcal{S}^{sh}_{tr,tr} = \mathcal{S}^{sh}_{12,12} + \mathcal{S}^{sh}_{13,13} + 2\mathcal{S}^{sh}_{12,13} = \mathcal{T}(1 - \mathcal{T})$, which gives the Lesovik formula.

In the system, having triangular symmetry, the eigenstates $E_0 = -2$ and $E_{\pm} = 1$ (with the wavevector $k = 0$ and $k = \pm 2\pi/3$) play a different role in the transport, which is seen in the bond conductances and the shot noise components. An electron wave injected with energy close to $E_0$ is perfectly split into both branches of the ring and the current cross-correlation function $\mathcal{S}^{sh}_{12,13}$ is positive. At the resonance $E_0$, the transmission $\mathcal{T} = 1$ and all correlation functions $\mathcal{S}^{sh}_{12,12} = \mathcal{S}^{sh}_{13,13} = \mathcal{S}^{sh}_{12,13} = 0$, which means that the bond currents are uncorrelated. The magnetic flux changes quantum interference conditions and correlates the bond currents; the cross-correlation $\mathcal{S}^{sh}_{12,13}$ becomes negative at the resonance and fully compensates the positive auto-correlation components $\mathcal{S}^{sh}_{12,12}$ and $\mathcal{S}^{sh}_{13,13}$ (with $\mathcal{S}^{sh}_{tr,tr} = 0$).

Quantum interference plays a crucial role in transport through the degenerate states at $E_{\pm} = 1$, where one can observe Fano resonance with destructive interference. In this region, the circular current $I^{dr}$ can be driven by the bias voltage. The bond conductances have an opposite sign, their maximal value is inversely proportional to the coupling, $\Gamma_{\alpha}$, with the electrodes, and they can be larger than unity. The direction of $I^{dr}$ depends on the bias voltage and the position of the Fermi energy $E_F$, with respect to the degenerate state $E_{\pm}$. The auto-correlation functions $\mathcal{S}^{sh}_{12,12}$, $\mathcal{S}^{sh}_{13,13}$ are large (inversely proportional to $\Gamma^2_{\alpha}$) close to the resonance. The cross-correlator $\mathcal{S}^{sh}_{12,13}$ is negative in the presence of the driven circular current. Our calculations show that a small magnetic flux, $\phi = 2\pi/16$, can destroy the Fano resonance, and two resonance peaks (with $\mathcal{T} = 1$) appear. The driven component, $I^{dr}$, is reduced with an increase of $\phi$, and it disappears at $\phi = 2\pi/4$. However, quantum interference still plays a role; the bond currents are strongly correlated (with large $\mathcal{S}^{sh}_{12,12}$ and $\mathcal{S}^{sh}_{13,13}$ and negative $\mathcal{S}^{sh}_{12,13}$). For a large coupling, the driven part $I^{dr}$ can be large and can profoundly modify the total circular current $I^c = I^{dr} + I^{\phi}$.

We also performed calculations of the bond currents and their correlations for rings with a various number of sites; in particular, for the benzene ring in para-, metha-, and ortho-connection with the electrodes. The results are qualitatively similar to those presented above for the 3QD ring: Quantum interference of the travelling waves with the eigenstates of opposite chirality leads to the driven circular currents, accompanied by large current fluctuations with a negative cross-correlation

component. To observe this effect, the two conducting branches should be asymmetric; in particular, in the benzene ring, the driven circular current appears for the metha- and ortho-connections, but is absent in the para-connection, where both conducting branches are equivalent (see also [7]).

An open problem is including interactions between electrons into the calculations of the coherent transport and shot noise. Coulomb interactions can be taken into account in the sequential regime [52], or by using the real-time diagrammatic technique [53–55]; however, in practice, one includes only first- and second-order diagrams with respect to the tunnel coupling and the role of QI is diminished. In principle, one can treat QI on an equal footing with electron interactions in the framework of quantum field theory [56], as was done for the Anderson single impurity model, by means of full counting statistics (FCS), where the average current and all its moments were calculated [57]. However, this is a formidable task, even for the simple 3QD model.

**Appendix A. Coupling to Atomic Chain Electrodes: Analytical Results**

The results for the conductances and shot noise may be simplified when we take all hopping integrals equal to $t$, the same position of the site levels $\varepsilon = 0$, and the symmetric coupling $t_L = t_R = t$, with the electrodes as a semi-infinite atomic chain. In this case, the Green functions in the electrodes are $g^r = e^{ik}/t$ and $g^a = e^{-ik}/t$ and the electron spectrum is $E_k = 2t\cos k$. From Equations (7)–(10), one can calculate the dimensionless bond conductances as

$$\mathcal{G}_{12}^L = 2\sin k\left[\sin k + \sin 3k - \sin(2k + \phi)\right]/A, \tag{A1}$$

$$\mathcal{G}_{12}^R = 2\sin k\left[\sin k + \sin 3k - \sin(2k - \phi)\right]/A, \tag{A2}$$

$$\mathcal{G}_{13}^L = 2\sin k\left[\sin k - \sin(2k - \phi)\right]/A, \text{ and} \tag{A3}$$

$$\mathcal{G}_{13}^R = 2\sin k\left[\sin k - \sin(2k + \phi)\right]/A, \tag{A4}$$

where the denominator

$$A = 4 + \cos 2\phi - 2\cos\phi(3\cos k - \cos 3k) - \cos 4k. \tag{A5}$$

It is seen an asymmetry with respect to the direction of the magnetic flux (to $\phi$) for the conductances $\mathcal{G}_{ij}^L$ and $\mathcal{G}_{ij}^R$ from the left and the right electrode. The transmission, $\mathcal{T}$, is expressed as

$$\mathcal{T} \equiv \mathcal{G}_{12}^L + \mathcal{G}_{13}^L = \mathcal{G}_{12}^R + \mathcal{G}_{13}^R = \mathcal{G}_{12} + \mathcal{G}_{13} = 2\sin^2 k[1 - 4\cos k(\cos\phi - \cos k)]/A, \tag{A6}$$

where the driven part of the bond conductances are calculated using Equations (15) and (16)

$$\mathcal{G}_{12} = 4\sin^2 k\cos k(2\cos k - \cos\phi)/A, \tag{A7}$$

$$\mathcal{G}_{13} = 2\sin^2 k(1 - 2\cos\phi\cos k)/A, \text{ and} \tag{A8}$$

$$\mathcal{G}_\phi^L = \mathcal{G}_\phi^R = 2\sin\phi\sin k\cos 2k/A, \tag{A9}$$

and, from Equations (19) and (20), the part induced by the flux is

$$\mathcal{G}_\phi^L = \mathcal{G}_\phi^R = 2\sin\phi\sin k\cos 2k/A. \tag{A10}$$

It can be seen that the conductance $\mathcal{G}_{12}$ becomes negative at $k = \pi/2$ (i.e., when the circular current becomes driven).

The shot noise for the bond currents is expressed as

$$\mathcal{S}^{sh}_{12,12} = 4\sin^2 k \,|e^{\iota\phi}(\cos\phi - 2\cos k) + \cos 2k|^2 / A^2\,, \tag{A11}$$

$$\mathcal{S}^{sh}_{13,13} = 4\sin^2 k \,|\cos k - e^{\iota\phi}|^2 / A^2, \tag{A12}$$

$$\mathcal{S}^{sh}_{12,13} = -4\sin^2 k \left[2\cos\phi\cos k(\cos\phi - \cos k)^2 + \sin^2\phi\right]/A^2,\text{ and} \tag{A13}$$

$$\mathcal{S}^{sh}_{tr,tr} = \mathcal{T}(1-\mathcal{T}) = 4\sin^2 k(\cos\phi - \cos k)^2[1 - 4\cos k(\cos\phi - \cos k)]/A^2\,. \tag{A14}$$

Notice that the cross-correlation $\mathcal{S}^{sh}_{12,13}$ can be positive or negative in the laminar or the vortex regime, respectively.

## References and Note

1. Webb, R.A.; Washburn, S.; Umbach, C.P.; Laibowitz, R.B. Observation of h/e Aharonov-Bohm Oscillations in Normal-Metal Rings. *Phys. Rev. Lett.* **1985**, *54*, 2696–2699, doi:10.1103/PhysRevLett.54.2696. [CrossRef]
2. Ji, Y.; Chung, Y.; Sprinzak, D.; Heiblum, M.; Mahalu, D.; Shtrikman, H. An electronic Mach-–Zehnder interferometer. *Nature* **2003**, *422*, 415–418, doi:10.1038/nature01503. [CrossRef] [PubMed]
3. Cardamone, D.M.; Stafford, C.A.; Mazumdar, S. Controlling Quantum Transport through a Single Molecule. *Nano Lett.* **2006**, *6*, 2422–2426, doi:10.1021/nl0608442. [CrossRef]
4. Solomon, G.C.; Andrews, D.Q.; Hansen, T.; Goldsmith, R.H.; Wasielewski, M.R.; Van Duyne, R.P.; Ratner, M.A. Understanding quantum interference in coherent molecular conduction. *J. Chem. Phys.* **2008**, *129*, 054701, doi:10.1063/1.2958275. [CrossRef] [PubMed]
5. Ke, S.H.; Yang, W.; Baranger, H.U. Quantum-Interference-Controlled Molecular Electronics. *Nano Lett.* **2008**, *8*, 3257–3261, doi:10.1021/nl8016175. [CrossRef]
6. Donarini, A.; Begemann, G.; Grifoni, M. All-Electric Spin Control in Interference Single Electron Transistors. *Nano Lett.* **2009**, *9*, 2897–2902, doi:10.1021/nl901199p. [CrossRef]
7. Rai, D.; Hod, O.; Nitzan, A. Circular currents in molecular wires. *J. Phys. Chem. C* **2010**, *114*, 20583–20594, doi:10.1021/jp105030d. [CrossRef]
8. Hong, W.; Valkenier, H.; Mészáros, G.; Manrique, D.Z.; Mishchenko, A.; Putz, A.; García, P.M.; Lambert, C.J.; Hummelen, J.C.; Wandlowski, T. An MCBJ case study: The influence of $\pi$-conjugation on the single-molecule conductance at a solid/liquid interface. *Beilstein J. Nanotechnol.* **2011**, *2*, 699–713, doi:10.3762/bjnano.2.76. [CrossRef] [PubMed]
9. Guédon, C.M.; Valkenier, H.; Markussen, T.; Thygesen, K.S.; Hummelen, J.C.; van der Molen, S.J. Observation of quantum interference in molecular charge transport. *Nat. Nanotechnol.* **2012**, *7*, 305–309, doi:10.1038/nnano.2012.37. [CrossRef]
10. Lambert, C.J. Basic concepts of quantum interference and electron transport in single-molecule electronics. *Chem. Soc. Rev.* **2015**, *44*, 875–888, doi:10.1039/C4CS00203B. [CrossRef]
11. Liu, J.; Huang, X.; Wang, F.; Hong, W. Quantum Interference Effects in Charge Transport through Single-Molecule Junctions: Detection, Manipulation, and Application. *Accounts Chem. Res.* **2019**, *52*, 151–160, doi:10.1021/acs.accounts.8b00429. [CrossRef]
12. Nakanishi, S.; Tsukada, M. Large Loop Current Induced Inside the Molecular Bridge. *Jpn. J. Appl. Phys.* **1998**, *37*, L1400–L1402, doi:10.1143/JJAP.37.L1400. [CrossRef]
13. Nakanishi, S.; Tsukada, M. Quantum Loop Current in a C60 Molecular Bridge. *Phys. Rev. Lett.* **2001**, *87*, 126801, doi:10.1103/PhysRevLett.87.126801. [CrossRef] [PubMed]
14. Daizadeh, I.; Guo, J.X.; Stuchebrukhov, A. Vortex structure of the tunneling flow in long-range electron transfer reactions. *J. Chem. Phys.* **1999**, *110*, 8865–8868, doi:10.1063/1.478807. [CrossRef]
15. Xue, Y.; Ratner, M.A. Local field effects in current transport through molecular electronic devices: Current density profiles and local nonequilibrium electron distributions. *Phys. Rev. B* **2004**, *70*, 081404, doi:10.1103/PhysRevB.70.081404. [CrossRef]
16. Stefanucci, G.; Perfetto, E.; Bellucci, S.; Cini, M. Generalized waveguide approach to tight-binding wires: Understanding large vortex currents in quantum rings. *Phys. Rev. B* **2009**, *79*, 073406, doi:10.1103/PhysRevB.79.073406. [CrossRef]

17. Rai, D.; Hod, O.; Nitzan, A. Magnetic field control of the current through molecular ring junctions. *J. Phys. Chem. Lett.* **2011**, *2*, 2118–2124, doi:10.1021/jz200862r. [CrossRef]

18. Rai, D.; Hod, O.; Nitzan, A. Magnetic fields effects on the electronic conduction properties of molecular ring structures. *Phys. Rev. B* **2012**, *85*, 155440, doi:10.1103/PhysRevB.85.155440. [CrossRef]

19. Yadalam, H.K.; Harbola, U. Controlling local currents in molecular junctions. *Phys. Rev. B* **2016**, *94*, 115424, doi:10.1103/PhysRevB.94.115424. [CrossRef]

20. Nozaki, D.; Schmidt, W.G. Current density analysis of electron transport through molecular wires in open quantum systems. *J. Comput. Chem.* **2017**, *38*, 1685–1692, doi:10.1002/jcc.24812. [CrossRef] [PubMed]

21. Patra, M.; Maiti, S.K. Modulation of circular current and associated magnetic field in a molecular junction: A new approach. *Sci. Rep.* **2017**, *7*, 43343, doi:10.1038/srep43343. [CrossRef] [PubMed]

22. Cabra, G.; Jensen, A.; Galperin, M. On simulation of local fluxes in molecular junctions. *J. Chem. Phys.* **2018**, *148*, 204103, doi:10.1063/1.5029252. [CrossRef] [PubMed]

23. Moskalets, M.V. Temperature-induced current in a one-dimensional ballistic ring with contacts. *Europhys. Lett. (EPL)* **1998**, *41*, 189–194, doi:10.1209/epl/i1998-00129-8. [CrossRef]

24. Chung, V.S.W.; Samuelsson, P.; Buttiker, M. Visibility of current and shot noise in electrical Mach-Zehnder and Hanbury Brown Twiss interferometers. *Phys. Rev. B* **2005**, *72*, 125320, doi:10.1103/PhysRevB.72.125320. [CrossRef]

25. Büttiker, M.; Samuelsson, P. Interference of independently emitted electrons in quantum shot noise. *Ann. Phys.* **2007**, *16*, 751–766, doi:10.1002/andp.200710255. [CrossRef]

26. Pilgram, S.; Samuelsson, P.; Förster, H.; Büttiker, M. Full-Counting Statistics for Voltage and Dephasing Probes. *Phys. Rev. Lett.* **2006**, *97*, 066801, doi:10.1103/PhysRevLett.97.066801. [CrossRef]

27. Förster, H.; Pilgram, S.; Büttiker, M. Decoherence and full counting statistics in a Mach-Zehnder interferometer. *Phys. Rev. B* **2005**, *72*, 075301, doi:10.1103/PhysRevB.72.075301. [CrossRef]

28. Förster, H.; Samuelsson, P.; Pilgram, S.; Büttiker, M. Voltage and dephasing probes in mesoscopic conductors: A study of full-counting statistics. *Phys. Rev. B* **2007**, *75*, 035340, doi:10.1103/PhysRevB.75.035340. [CrossRef]

29. Bauerle, C.; Glattli, D.C.; Meunier, T.; Portier, F.; Roche, P.; Roulleau, P.; Takada, S.; Waintal, X. Coherent control of single electrons: A review of current progress. *Rep. Prog. Phys.* **2018**, *81*, 056503, doi:10.1088/1361-6633/aaa98a. [CrossRef] [PubMed]

30. Lesovik, G.B. Excess quantum noise in two-dimensional ballistic microcontacts. *Pis'ma Zh. Eksp. Teor. Fiz.* **1989**, *49*, 513–515.

31. Haug, H.; Jauho, A.P. *Quantum Kinetics in Transport and Optics of Semiconductors*; Springer: Berlin/Heidelberg, Germany, 2008, doi:10.1007/978-3-540-73564-9.

32. Blanter, Y.; Büttiker, M. Shot noise in mesoscopic conductors. *Phys. Rep.* **2000**, *336*, 1–166, doi:10.1016/S0370-1573(99)00123-4. [CrossRef]

33. Levitov, L.S.; Lesovik, G.B. Charge-transport statistics in quantum conductors. *Pis'ma Zh. Eksp. Teor. Fiz.* **1992**, *55*, 534–537.

34. Lesovik, G.B.; Sadovskyy, I.A. Scattering matrix approach to the description of quantum electron transport. *Physics-Uspekhi* **2011**, *54*, 1007–1059, doi:10.3367/UFNe.0181.201110b.1041. [CrossRef]

35. Martin, T.; Landauer, R. Wave-packet approach to noise in multichannel mesoscopic systems. *Phys. Rev. B* **1992**, *45*, 1742–1755, doi:10.1103/PhysRevB.45.1742. [CrossRef]

36. Jayannavar, A.M.; Singha Deo, P. Persistent currents in the presence of a transport current. *Phys. Rev. B* **1995**, *51*, 10175–10178, doi:10.1103/PhysRevB.51.10175. [CrossRef]

37. One can define the driven current as [7]: $I^{dr} = (I_{12}l_{12} - I_{13}l_{13})/(l_{12} + l_{13})$, where $l_{12}, l_{13}$ denotes the length of the upper and the lower branch. For $I_{13} \to 0$ one gets a finite circular current, what is an artefact.

38. Bułka, B.R. Current and power spectrum in a magnetic tunnel device with an atomic-size spacer. *Phys. Rev. B* **2000**, *62*, 1186–1192, doi:10.1103/PhysRevB.62.1186. [CrossRef]

39. Büttiker, M.; Stafford, C.A. Charge Transfer Induced Persistent Current and Capacitance Oscillations. *Phys. Rev. Lett.* **1996**, *76*, 495–498, doi:10.1103/PhysRevLett.76.495. [CrossRef]

40. Cedraschi, P.; Büttiker, M. Suppression of level hybridization due to Coulomb interactions. *J. Phys. Condens. Matter* **1998**, *10*, 3985–4000, doi:10.1088/0953-8984/10/18/009. [CrossRef]

41. Cedraschi, P.; Ponomarenko, V.V.; Büttiker, M. Zero-Point Fluctuations and the Quenching of the Persistent Current in Normal Metal Rings. *Phys. Rev. Lett.* **2000**, *84*, 346–349, doi:10.1103/PhysRevLett.84.346. [CrossRef]

42. Cedraschi, P.; Buttiker, M. Zero-point fluctuations in the ground state of a mesoscopic normal ring. *Ann. Phys.* **2000**, *289*, 165312, doi:10.1103/PhysRevB.63.165312. [CrossRef]

43. Semenov, A.G.; Zaikin, A.D. Fluctuations of persistent current. *J. Phys. Condens. Matter* **2010**, *22*, 485302, doi:10.1088/0953-8984/22/48/485302. [CrossRef]

44. Semenov, A.G.; Zaikin, A.D. Persistent current noise and electron-electron interactions. *Phys. Rev. B* **2011**, *84*, 045416, doi:10.1103/PhysRevB.84.045416. [CrossRef]

45. Semenov, A.G.; Zaikin, A.D. Persistent currents in quantum phase slip rings. *Phys. Rev. B* **2013**, *88*, 054505, doi:10.1103/PhysRevB.88.054505. [CrossRef]

46. Semenov, A.G.; Zaikin, A.D. Quantum phase slip noise. *Phys. Rev. B* **2016**, *94*, 014512, doi:10.1103/PhysRevB.94.014512. [CrossRef]

47. Moskalets, M. Persistent currents in ballistic normal-metal rings. *Low Temp. Phys.* **2010**, *36*, 982–989, doi:10.1063/1.3521568. [CrossRef]

48. Komnik, A.; Langhanke, G.W. Full counting statistics of persistent current. *Phys. Rev. B* **2014**, *90*, 165107, doi:10.1103/PhysRevB.90.165107. [CrossRef]

49. Saha, M.; Maiti, S.K. Circulating current in 1D Hubbard rings with long-range hopping: Comparison between exact diagonalization method and mean-field approach. *Phys. E Low-Dimens. Syst. Nanostruct.* **2016**, *84*, 118–134, doi:10.1016/j.physe.2016.05.042. [CrossRef]

50. Imry, Y. *Introduction to Mesoscopic Physics*; Oxford University Press: New York, NY, USA, 1997.

51. Cheung, H.F.; Gefen, Y.; Riedel, E.K.; Shih, W.H. Persistent currents in small one-dimensional metal rings. *Phys. Rev. B* **1988**, *37*, 6050–6062, doi:10.1103/PhysRevB.37.6050. [CrossRef]

52. Nazarov, Y.V.; Blanter, Y.M. *Quantum Transport: Introduction to Nanoscience*; Cambridge University Press: Cambridge, UK, 2009, doi:10.1017/CBO9780511626906. [CrossRef]

53. Schoeller, H.; Schön, G. Mesoscopic quantum transport: Resonant tunneling in the presence of a strong Coulomb interaction. *Phys. Rev. B* **1994**, *50*, 18436–18452, doi:10.1103/PhysRevB.50.18436. [CrossRef]

54. König, J.; Schmid, J.; Schoeller, H.; Schön, G. Resonant tunneling through ultrasmall quantum dots: Zero-bias anomalies, magnetic-field dependence, and boson-assisted transport. *Phys. Rev. B* **1996**, *54*, 16820–16837, doi:10.1103/PhysRevB.54.16820. [CrossRef]

55. Thielmann, A.; Hettler, M.H.; König, J.; Schön, G. Cotunneling Current and Shot Noise in Quantum Dots. *Phys. Rev. Lett.* **2005**, *95*, 146806, doi:10.1103/PhysRevLett.95.146806. [CrossRef] [PubMed]

56. Kamenev, A. *Field Theory of Non-Equilibrium Systems*; Cambridge University Press: Cambridge, UK, 2011, doi:10.1017/CBO9781139003667. [CrossRef]

57. Gogolin, A.O.; Komnik, A. Towards full counting statistics for the Anderson impurity model. *Phys. Rev. B* **2006**, *73*, 195301, doi:10.1103/PhysRevB.73.195301. [CrossRef]